JOURNAL OF AIRCRAFT
Vol. 47, No. 5, September–October 2010

Joined-Wing Wind-Tunnel Test for Longitudinal Control via Aftwing Twist

Vanessa L. Bond*
Arnold Engineering Development Center, Arnold Air Force Base, Tennessee 37389
Robert A. Canfield†
Virginia Polytechnic Institute and State University, Blacksburg, Virginia 24061
Maria da Luz Madruga Santos Matos‡
Academia da Força Aérea, 2710 Sintra, Portugal
Afzal Suleman§
University of Victoria, Victoria, British Columbia V8W 3P6, Canada
and
Maxwell Blair¶
U.S. Air Force Research Laboratory, Wright Patterson Air Force Base, Ohio 45433

DOI: 10.2514/1.41140

Wind-tunnel tests were conducted to assess the use of aftwing twist for longitudinal control in a joined-wing aircraft. Forces and moments required for pitch control were measured experimentally, along with limited chordwise pressure measurements. Comparisons of aerodynamic panel model predictions with experimental data were used to calculate camber and center-of-pressure corrections. The lift-curve slope measured at four flow speeds compared favorably to linear predictions over the range of 20° angles of attack. The pitching moment coefficient was linear at the three lower flow speeds for untwisted and twist-down aft wings over a narrower range of about 10° angles of attack. The pressure exhibited shifts in the chordwise distribution at angles of attack coinciding with the change in the moment curve slope. The large spread in the twist-up aftwing configuration drag and pitching-moment coefficients indicated flow separation on the aft wing, even at small angles of attack, deterring the twist effectiveness. Independent forward and aftwing measurements and more extensive use of pressure sensors are recommended in future experiments to confirm the apparent separation and interference effects that must be avoided if aftwing twist is to be used for pitch control on a joined wing.

Nomenclature

b	=	wing semichord, wing semispan
$C_{L(\text{roll})}$	=	rolling coefficient of moment
C_{Lt}	=	coefficient of lift of tail
$C_{L\alpha}$	=	coefficient of lift with respect to angle of attack
C_M	=	pitching coefficient of moment
C_{Mcg}	=	coefficient of moment at the center of gravity
C_{Mo}	=	coefficient of moment at zero lift
C_N	=	yawing coefficient of moment
c	=	mean aerodynamic chord
D	=	drag
F_x	=	X component of the resultant pressure force acting on the vehicle
F_z	=	Z component of the resultant pressure force acting on the vehicle
L	=	lift
M	=	mass primary quantity
M_x	=	X component of moment acting on the vehicle
M_y	=	Y component of the moment acting on the vehicle
M_z	=	Z component of the moment acting on the vehicle
p	=	total pressure
q_∞	=	dynamic pressure
Re	=	Reynolds number
S_{mod}	=	wing area for the model
V	=	velocity
α	=	angle of attack
δ_e	=	angle of elevator deflection
θ	=	angle of twist, pitch (with subscript)
μ	=	viscosity, aeroelastic mass
ρ_∞	=	air density

Subscripts

m	=	pertaining to the wind-tunnel model
w	=	pertaining to the aircraft (wing)

Presented as Paper 2007-1772 at the 48th AIAA/ASME/ASCE/AHS/ASC Structures, Structural Dynamics, and Materials Conference, Honolulu, HI, 23–26 April 2007; received 21 September 2008; revision received 23 February 2010; accepted for publication 24 February 2010.

*Commander, 716th Test and Evaluation Squadron. Member AIAA.
†Professor of Aerospace Engineering. Associate Fellow AIAA.
‡Professor of Aeronautical Engineering. Member AIAA.
§Professor of Mechanical Engineering. Member AIAA.
¶Senior Aerospace Engineer. Associate Fellow AIAA.

I. Introduction

THE joined-wing sensorcraft (Fig. 1) is unique in two major areas [1]. First, it is an aircraft built around its sensors; that is, the sensors are built into the composite skin. The second unique aspect of this design is provided by the joined-wing configuration. To maximize the usable wing surface area for the sensors, and avoid interference with the sensors, control surfaces should be minimized or eliminated. Minimizing the control surfaces takes advantage of the Wolkovitch effect of the joined-wing configuration [2]. Unlike a conventional planform, wing bending acts in the plane connecting the fore and aft wings. To resist this bending, the wing box structure should separate the forward and aft spars as far as possible (Fig. 2). Therefore, conventional control surfaces should be avoided, since the beneficial feature of maximizing the distance between forward and rear spars leaves little room for leading- and trailing-edge control surfaces. Additionally, eliminating control surfaces minimizes

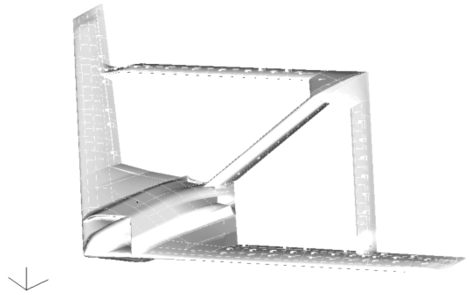

Fig. 1 Boeing joined-wing SensorCraft.

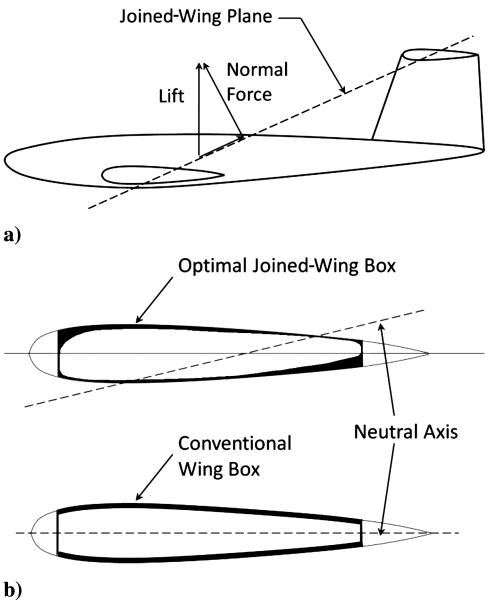

Fig. 2 Joined-wing effects: a) tilted bending plane and b) optimum wing box material distribution [12].

interference with the sensor array, resulting in a more effective system. To achieve the longitudinal control objective, the composite wing subjected to flexible aftwing twist was considered. Initial experiments were conducted to determine whether the twisted aft wing could produce the forces and moments required for pitch control.

Wolkovitch, who first introduced the joined-wing concept in patents in the 1970s, published an overview in 1986 [2]. More detailed aerodynamic and structural studies by Kroo et al. [3] have confirmed the Wolkovitch effect [2] and defined some characteristics of joined-wing structures that are advantageous to the design. Later, Smith et al. continued their research and built a demonstrator joined-wing aircraft [4]. In addition, Tyler et al. of the U.S. Air Force Research Laboratory (AFRL) completed complementary computational fluid dynamics (CFD) and wind-tunnel examinations [5] of an AFRL-generated joined-wing configuration. Corneille and Franke tested several configurations of joined wings [6] in the wind tunnel at the Air Force Institute of Technology (AFIT). The flexible aftwing twist concept modeled by Blair et al. [7] was investigated in the experiments reported here.

II. Theoretical Formulation

A. Aerodynamic Wind-Tunnel Testing Theory

Before testing a full-scale article in an uncontrolled environment, a scaled model can be used to gather valuable data from wind-tunnel testing under controlled conditions. Not only does this testing reduce cost and mitigate risk to aircraft development, it allows the engineer to control many of the variables associated with flight testing an aircraft. In this way, innovative designs and theories put to practice can be evaluated in a controlled environment with less uncertainty.

An aerodynamic model that is tested under the same Reynolds and Mach numbers will have the same force and moment coefficients as the full-scale aircraft [8]. In this study, Mach and Reynolds numbers could not be matched due to the low speed of the wind tunnel and model-size limitations. It is generally accepted that compressibility effects can be neglected below Mach 0.4 [8]. In addition, with Reynolds numbers above 4×10^5, the oscillatory air forces associated with the Reynolds number are relatively small [9]. Thus, the flutter speed and frequency are relatively unaffected by Reynolds number disparities. Moreover, above $Re = 1.5 \times 10^6$, the boundary-layer effects are predictable. However, the Reynolds number in this study is close to critical, leading to some inconsistency in the collected data due to Reynolds number effects. Nevertheless, the data collected are still relevant, considering that future sensorcraft concepts are relying upon swept-wing laminar flow control [1].

In addition to directly measuring the forces and moments using a balance, pressure measurements were collected in the wind tunnel. For this joined-wing configuration, the majority of the lift comes from the forward wing, since it is the largest. The lift produced by the aft wing, however, is also of interest, because this is the surface that will be manipulated to control pitch. Therefore, special attention was paid to changes in lift due to the aft wing with various twist angles.

B. Conventional and Wing Twist Stability Derivatives

Conventional aircraft use an elevator or similar control surface on the horizontal tail to change lift and, in turn, effect a change in the coefficient of moment at a zero angle of attack, C_{M_0}, to keep the aircraft trimmed at different speeds. The range of required control-surface deflection to provide longitudinal control of the aircraft must also be determined for the joined-wing aircraft. In this case, however, the objective is to determine how much twist is required of the aft wing, rather than a control-surface deflection, to provide longitudinal control of the aircraft. This can be accomplished by determining the moment curve slope, $\partial C_M/\partial\theta$, for changes in twist θ.

For a conventional aircraft, the moment curve slope $\partial C_M/\partial\alpha$ remains constant, but the curve shifts down as the elevator δ_e is deflected downward (positive by convention) for a given angle of attack. Plotting C_L or C_m vs δ_e at a constant angle of attack, the curves would have a significant linear region for most conventional aircraft (Fig. 3). For the joined wing, elevator deflection δ_e is replaced with aftwing twist θ. The moment curve can then be used to measure how well the twist controls the pitch of the aircraft. The moment referred to includes both lifting surfaces (fore and aft wings). Like elevator deflection, where down is positive, positive will be designated as aftwing trailing-edge down and aftwing leading-edge up, henceforth referred to as twist up. Conversely, negative twist, referred to as twist down, means the aftwing leading edge moves downward. Since the aft wing will be twisted, it is possible that this joined wing may not have a constant $\partial C_{Mcg}/\partial\alpha$ for various angles of twist, as with a conventional wing.

C. Scaling Laws

There are three primary ratios that must be considered for scaling the aeroelastic characteristics of the full-scale joined wing. These ratios capture the critical parameters used in scaling the aeroelastic model and are based on physical limitations of a particular test setup.

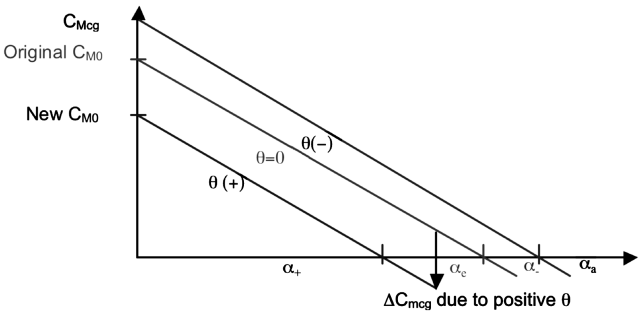

Fig. 3 Theoretical effect of aftwing twist on moment coefficient [13].

These ratios include characteristic length ratio, air density ratio, and velocity ratio. The length ratio is established by the size of the full-scale vehicle compared with wind-tunnel restrictions. For this study, it is defined as

$$\frac{b_m}{b_w} = \frac{1}{38} \tag{1}$$

where m and w are reduced (model) scale and full scale, respectively.

The standard day altitude of the wind tunnel and the mission profile fixes the air density ratio:

$$\frac{\rho_{\infty m}}{\rho_{\infty w}} = \frac{\rho_{\infty 165m}}{\rho_{\infty 15240m}} = 6.63 \tag{2}$$

The velocity ratio is fixed by the maximum viable speed of the wind tunnel and the mission profile:

$$\frac{V_m}{V_w} = \frac{50 \text{ m/s}}{177 \text{ m/s}} = 0.2825 \tag{3}$$

III. Approach

A. Wind-Tunnel Model Design and Research Requirements

As mentioned in Sec. II, one of the primary considerations for scaling the aerodynamic characteristics of the full-scale article is matching the Reynolds number. In addition, there are real-world limitations that must be taken into account, such as the size and speed of the wind tunnel, the instrumentation used, and the ability to produce an accurate model at the final scale factor.

The scale of the test model was determined primarily by the physical constraints of the Göttingen Wind Tunnel at the Portuguese Air Force Academy, where the tests were accomplished. The tunnel was used in an open test-section configuration with a cross section of $1.2 \times 0.8 \times 2$ m. To avoid turbulence, the usable test area must maintain uniform flow velocity (less than 0.8% in pressure variation), limiting the testable area to $1.1 \times 0.6 \times 1.4$ m. A six-degree-of-freedom Schenck wind-tunnel force balance was used to measure the forces and moments experienced by the model, which dictated that the wing be mounted vertically. With these constraints, the wind-tunnel model was limited to 0.6 m for half-span. The length from the nose to the tip of the tail boom was 65% of the full span, or 0.776 m for the scaled model. For the full-size model, the distance from the nose to the center-of-gravity (c.g.) location was 24.5% of the span, or 0.293 m on the scaled model. The MSC/Nastran panel model for the full scale predicted an aircraft neutral point less than 2.54 cm aft of the c.g. The corresponding neutral point on the scaled model was 0.294 m aft of the nose: a distance of 24.5% of span. The scaled model was mounted on the Schenck balance, 6.5 cm aft of the scaled c.g. location, or 0.358 m aft of the nose.

The joined-wing sensorcraft model was sized appropriately for a 0.6 m half-span, resulting in a 1:38 scale model. Recent experience with this wind tunnel has shown that this size of model will remain outside the shear layer induced by the wind tunnel at flow velocities up to 50 m/s. The test velocities were approximately 20, 30, 40, and 50 m/s. At the lower speed, however, it was anticipated that the pressure sensors would be unable to record valid data. The usable pressure data test conditions were 30, 40, and 50 m/s. As mentioned, the highest velocity that will produce flow without disruption from the shear layer induced by the wind tunnel is 50 m/s. Thus, this was the final speed.

With the given constraints, it was not possible to match the Reynolds number in this wind tunnel. Nevertheless, a CFD model can be calibrated to the wind-tunnel results at their Reynolds numbers. To calculate Reynolds numbers, the following equation was used with the forewing mean aerodynamic chord (MAC) as the characteristic length:

$$Re = \frac{\rho_\infty V c}{\mu} \tag{4}$$

The values in Table 1 illustrate that the Reynolds numbers of the wind-tunnel testing and the full-scale aircraft differ by an order of magnitude. As mentioned in Sec. II, the Reynolds number effects may account for the high drag measured during testing, since the wind-tunnel model Reynolds number is near the critical Reynolds number of 5×10^5.

In designing the wind-tunnel model, the measurement requirements were taken into account. Lift, drag, and side force coefficients were measured by the Schenck wind-tunnel force balance, which also dictated that the half-span model be mounted vertically (Fig. 4). The right half-span was chosen arbitrarily. The following equations were used to transform the forces:

$$L = F_x \sin\alpha + F_z \cos\alpha \tag{5}$$

$$D = -F_x \cos\alpha + F_z \sin\alpha \tag{6}$$

where F_x and F_z are the components of the resultant pressure force acting on the vehicle measured by the Schenck balance, and α is the angle of attack.

As mentioned previously, this study made use of an existing design, supplied as a finite-element model (FEM) by the sensorcraft program office for the purpose of mitigation risk to their program. The FEM was used to create the shape of the wind-tunnel model, both in the nominal configuration and also with $\pm 15°$ of aftwing twist. The forward wing used a 10% thickness-to-chord airfoil and the aft wing a 17% thick airfoil. Forward and aftwing ribs from the FEM in Fig. 5 depict the approximate airfoil shape. Structural modifications were made to the FEM to enable a twisted aft wing, and then the outer-mold line (OML) of the twisted configurations was used to create the wind-tunnel shapes.

The $\pm 15°$ values of the aftwing twist were chosen based on calculations for pitch control on the AFIT-designed wing, for which the aftwing twist ranged from -10 to $5°$ for trimmed flight throughout the mission profile [10], although it is an otherwise arbitrary value for the purpose of this design. To reduce the force required to achieve wing twist, simulating a realizable actuator, the aftwing FEM was modified in two ways. First, a slit was made spanwise in the skin of the aft wing to allow for a more unrestricted twist (Fig. 6). Then, the ribs of the FEM were modified from a solid plane to a three-sided frame design (Fig. 5b) to reduce torsional stiffness. The extent of these structural modifications is rather lengthy and documented in another paper [11]. These modifications allowed for the use of a 49,856 N actuator to achieve 15° of change in the control-surface angle, which is less than that used in a Boeing F-15 Eagle elevator actuator at 124,550 N [11]. The wind-tunnel model was not designed to twist dynamically but to have a fixed twist built into the rigid model. Therefore, to accomplish the required test objectives, three different wind-tunnel model configurations were required. The OML of the nominal wing (no twist) and resulting wing

Table 1 Reynolds number comparison for wind tunnel and full-scale aircraft

	Wind-tunnel testing	Full-scale aircraft loiter	Full-scale aircraft ingress/egress
V_i (m/s)	50	118	177
Mach no.	0.15	0.4	0.6
MAC, m	0.0968	3.68	3.68
ρ, kg/m^3	1.19	0.092	0.188
μ, Pa · s	1.78×10^{-5}	1.42×10^{-5}	1.42×10^{-5}
Re	3.23×10^5	2.80×10^6	8.62×10^6

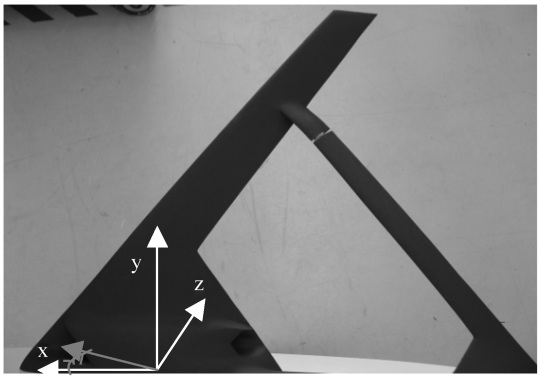

Fig. 4 Wind-tunnel model with nominal aft wing.

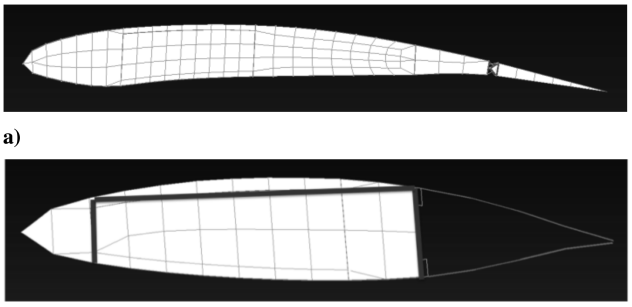

Fig. 5 Ribs: a) forward wing, and b) aftwing (flexible frame modification highlighted).

twisted up and down 15° were given to a CAD modeler to make detailed drawings, from which the wind-tunnel models were fabricated.

The wind-tunnel models were fabricated from foam, balsa wood, and fiberglass. Placement of the pressure ports was also finalized during fabrication and was complicated by the small size of the 1:38 scale model. The leading-edge-down twist configuration is illustrated in Fig. 7. This depicts the FEM prediction of the OML of the wing twisted down 15°. The primary area of twist occurs at the root, which is expected, given the location of the actuation force is a coupled force at the aftwing-tail joint (Fig. 6).

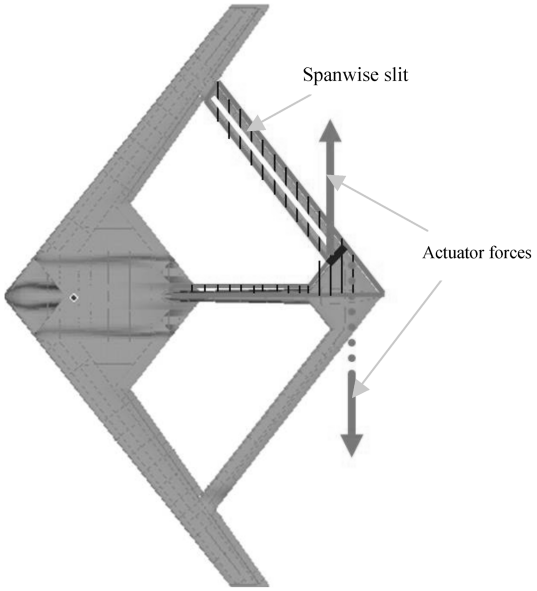

Fig. 6 Aft wing with spanwise slit (not to scale).

Fig. 7 Aftwing twist-down configuration with spanwise slit.

Because of the complexity of the design, it was decided to build one model with a reconfigurable aft wing. The nominal aft wing could be replaced by either of the twisted (15° up or down) aft wings (Fig. 8).

B. Wind-Tunnel Testing

A Schenck force balance was used to measure the forces and moments in the x, y, and z directions (see Fig. 4). The model was mounted on a platform that sat on top of the Schenck scale. The platform had a disk cutout, such that the model could be rotated to new angles of attack without adjusting the wind-tunnel conditions.

Testing was accomplished in the Portuguese Air Force Academy's Göttingen Wind Tunnel. The closed-circuit horizontal tunnel was used in the open test-section configuration, a contraction ratio of 1:5.53, and a test velocity range from 5 to 70 m/s.

Pressure measurements were taken from a single span location on each of the front and aft wings. The location was chosen halfway between the joint and root on each wing to minimize flow interaction from another surface. Figure 9 depicts the approximate cross-sectional locations of these ports, while Table 2 lists the exact locations with respect to the leading edge of each wing.

Each of the 18 pressure ports were connected to two pressure transducers via NetScanner Model 9016 Ethernet Intelligent Pressure Scanners to acquire the 18 discrete measurements. The system was connected to a National Instruments data acquisition system that, in turn, was connected to a personal computer, used to run LabVIEW software and record the data.

Before operating the wind tunnel, the ambient values of the forces and moments were recorded at each angle of attack. The force and moment measurements were taken until each was within 0.05 N or N · m, respectively. Once this tare was recorded, the data acquisition systems were configured for the test run.

For wind-tunnel operation, the outside air pressure was recorded for use in determining the dynamic pressure of the test run. The tunnel was turned on and adjusted to the speed required for the data capture. The wind-tunnel air flow temperature was monitored until

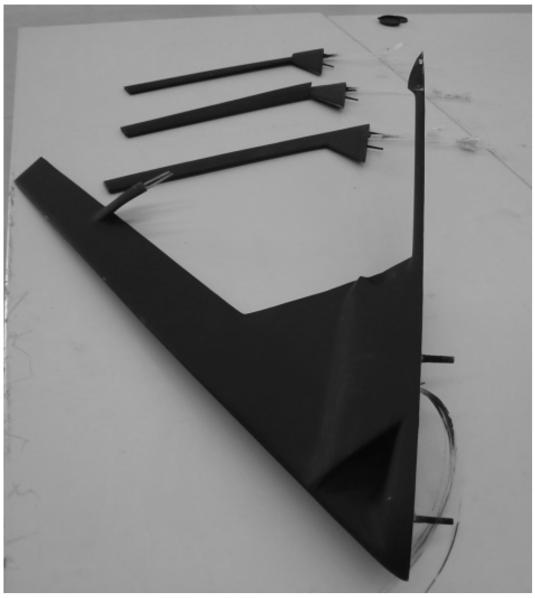

Fig. 8 The 0.6 m half-span model with nominal, 15 down, and 15 up (front to back) twisted aft wings.

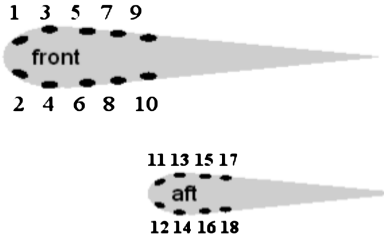

Fig. 9 Pressure port locations of fore and aft wings.

the temperature was stable, indicating steady flow and readiness for test.

Once the desired angle of attack was set, two to three force and moment measurements were typically recorded, while pressure data were simultaneously collected. Then, the angle of attack was incremented by 1° and the process repeated. This process was repeated at each airspeed for each configuration: nominal and ±15° aft wing. The test matrix is outlined in Table 3.

Initial flow visualization testing was accomplished in an attempt to show stall characteristics. Although testing was accomplished through a wide range of angles of attack, stall was not apparent. The vertical offset between forward and aftwing roots produced a joint angle (forewing dihedral plus aftwing anhedral) of approximately 16° (Fig. 10).

Each configuration, nominal, twist up, and twist down was tested at varied conditions, given in Table 3. Since the focus of this study is on pitch control, changes in the angles of attack were the primary focus. Testing was accomplished, for the most part, at angles of attack from −15 to +15°, in 1° increments.

IV. Results and Discussion

As mentioned in Sec. III, the wind-tunnel test was completed to demonstrate the use of wing twist for longitudinal (pitch) control in a joined-wing-aircraft configuration and to validate models that are used in analysis methods. The forces and moments required for pitch control and pressure measurements were recorded in the experiment. The following discussion focuses on pitch control but also highlights some characteristics worthy of note based on these tests.

A. Computational and Experimental Test Force and Moment Results

Most important to this portion of the study was determination of aerodynamic forces such that pitch control is realizable. Not only does coefficient of pitching moment C_{My} come into play to demonstrate wing twist effectiveness but also to determine features such as the usable angle-of-attack range before separation occurs and the possible contribution from Reynolds numbers (that may be not equivalent to the full-scale FEM).

Table 2 Port position percent of chord relative to the leading edge

Port number[a]	Forewing position, %	Port number[a]	Aftwing position, %
1/2	5	11/12	6
3/4	16	13/14	17
5/6	28	15/16	29
7/8	40	17/18	40
9/10	52		

[a]Odd port numbers are on top of the wing and even are on the bottom.

Table 3 Wind-tunnel test matrix

Aftwing twist, deg	Velocity, m/s	Angle of attack, °
Nominal	20, 30, 40, 50	−15 to +15
+15	20, 30, 40, 50	−15 to +15
−15	20, 30, 40, 50	−15 to +15

Fig. 10 Sixteen degrees of offset between the front and aft wings.

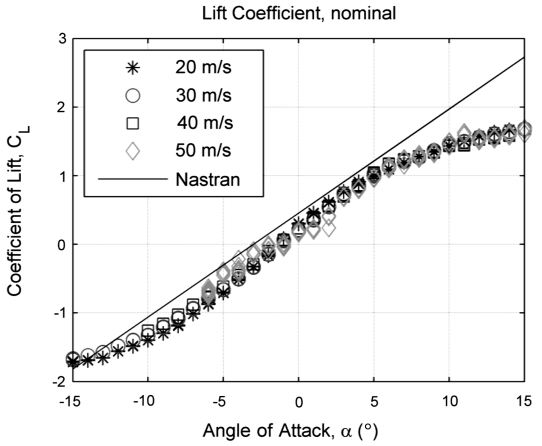

Fig. 11 Lift curves for nominal aftwing configuration.

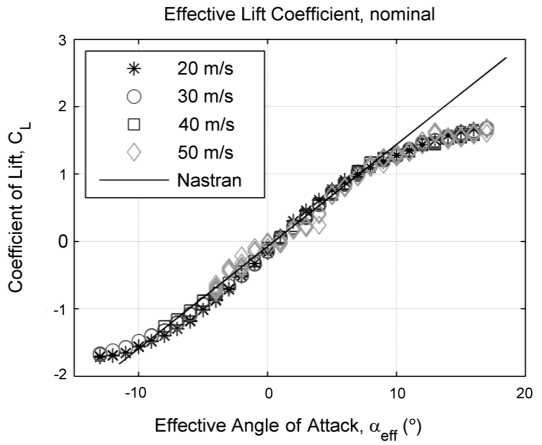

Fig. 12 Experimental lift and computational lift adjusted for zero-lift angle of attack.

Since the data are normalized and put in coefficient form, the $C_{L\alpha}$ curves are consistent for the various airspeeds in the nominal aftwing configuration (Fig. 11). The computational results produced in MSC/Nastran from the aerodynamic panel model were also reasonably consistent with the experimental data within the linear regime (Fig. 11). However, since camber and thickness were not modeled in MSC/Nastran, zero lift occurs at a −2° angle of attack for the experimental data and a −3.5° angle of attack for the computational results. When the lift coefficient was plotted, such that zero lift occurred at a zero angle of attack, the computational results matched experimental data in the linear regime (Fig. 12). Stall appeared to occur outside of −13 and +18° effective angles of attack.

While the lift curves were fairly consistent, the wing twist effectiveness was inconsistent at the higher speed (Fig. 13), likely due to turbulent transition. Reynolds number effects are not evident for the lift in Fig. 12, probably because most of the lift comes from the forward wing, where the laminar-to-turbulent transition may not have occurred, while transition may have occurred at 50 m/s on the aft wing. In Fig. 13, the moment curve at 50 m/s departs from the moment curves at lower speeds in a markedly nonlinear fashion. A large spread in repeated measurements is evident at some angles of attack for 50 m/s in Fig. 13 and the following figures. Otherwise, the measurements were repeatable, showing little variation for a given

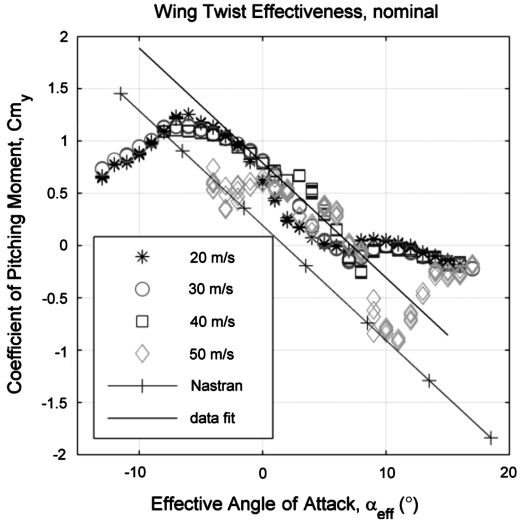

Fig. 13 Wing twist effectiveness for nominal aftwing configuration adjusted for zero-lift angle of attack.

speed, angle of attack, and twist. For this reason, the following plots focus on 30 m/s results in Figs. 14–21, where the repeated measurements demonstrated low variation. The maximum (over angle of attack) standard deviations, maximum values, and minimum values are given in Table 4 for the repeated measurements at each set of configuration parameters.

The computational results produced in MSC/Nastran from the panel model, after correction for a zero-lift angle of attack, still show a discrepancy in moment coefficient relative to a linear data fit to the experimental results (curve labeled data fit in Fig. 13). The difference can be calculated by

$$\Delta C_{My} = (\Delta C_{My})_m - (\Delta C_{My})_w = \left(\frac{d}{c}C_L\right)_m - \left(\frac{d}{c}C_L\right)_w \tag{7}$$

where c is the chord of the forward wing (subscripts w and m represent the full-scale and subscale models, respectively) and d is the moment arm used to calculate the pitching moment C_{My} of the vehicle to include both wings. Based on the aforementioned exercise of aligning the full-scale (computational) and subscale wind-tunnel results, $(C_L)_m = (C_L)_w$. Thus, Eq. (7) can be simplified:

$$\Delta C_{My} = C_L\left[\left(\frac{d}{c}\right)_m - \left(\frac{d}{c}\right)_w\right] \tag{8}$$

A correction factor moment arm Δd can be applied to equate the computational-to-experimental pitching moment coefficient, $d_{\text{corrected}} = d_w + \Delta d_w$, such that

$$\left(\frac{d+\Delta d}{c}\right)_w = \left(\frac{d}{c}\right)_m \tag{9}$$

Substituting Eq. (9) into Eq. (8) and solving for the correction factor moment arm on the full-size joined wing, using the experimental data at the $-1.5°$ angle of attack, we may solve for the center-of-pressure correction length:

$$\Delta d_w = c_w\frac{\Delta C_{My}}{C_L} = 3.68\text{ m}\left(\frac{0.5985}{-0.3028}\right) = -7.27\text{ m} \tag{10}$$

This is evidence of the need for experimental results, since this correction factor can be applied to future computational models. The sign convention of the correction factor moment arm is consistent with the angle of attack. This is a significant center-of-pressure correction: nearly two MAC lengths. Thus, modeling camber in MSC/Nastran may be important for predictions.

Figure 14 displays the expected behavior, whereby twist up shifts the moment curve down. However, the deflection of the twist-down aftwing configuration was not as continuous as the nominal and twist-up configurations. For instance, Fig. 14 indicates a 71% change in pitching moment for the twist-down configuration between 5 and 6°, whereas the change between 4 and 5° is only 22%. As will be seen, interference and separation effects were evident between the -5 and $+5°$ angles of attack for the twist-down condition. Outside this angle-of-attack range, the twist down does shift the moment curve up.

Figure 15 shows that drag rises drastically above the $-5°$ angle of attack for twist down. Examination of the high and erratic values of axial force in Fig. 16, from a -5 to a 10° angle of attack for twist down, suggests that there is a breakdown in the flow due to separation at these low angles of attack. The separation may be due to interference from the forewing flow impinging on the aft wing. Also, a

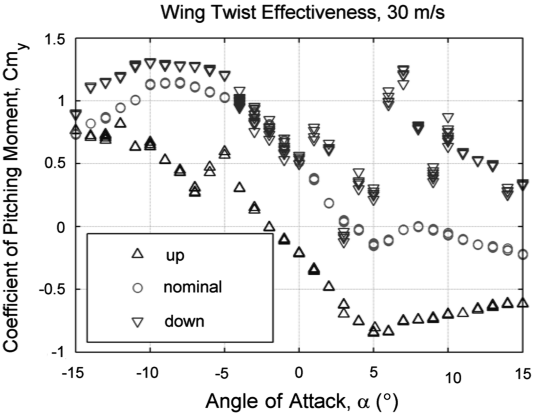

Fig. 14 Twist effectiveness for twist up, down, and nominal configurations.

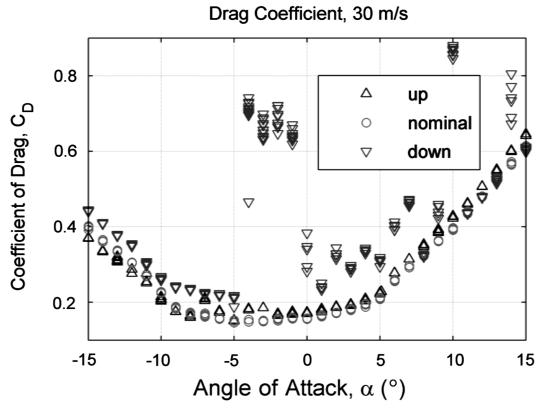

Fig. 15 High drag at low angles of attack in the twist-down configuration.

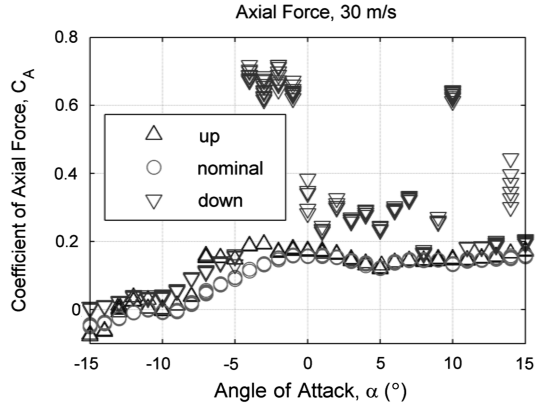

Fig. 16 Separation onset at low angle of attack.

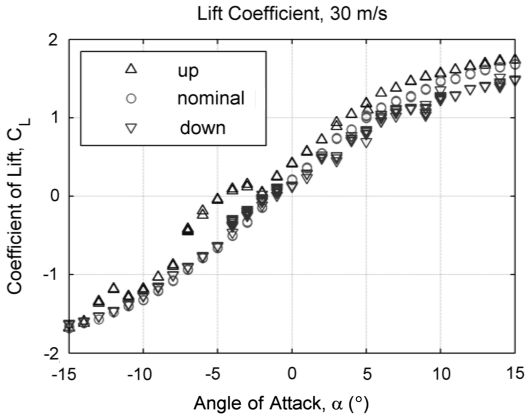

Fig. 17 Lift curves for twist up, down, and nominal configurations.

noticeable break in the OML at the root (Fig. 7) to allow freedom of movement of the aft wing may contribute to flow separation there. A shroud, planned for later models, could decrease the drag, especially noticeable in Fig. 15, for the twist-down configuration.

Departure of the lift curve for the twist-up configuration below a −2° angle of attack in Fig. 17 may also indicate interference effects. The improved lift in this region accounts for the corresponding higher lift-to-drag ratio for twist up at these angles of attack in Fig. 18. The overall higher lift for twist up in both figures is due to the additional lift generated on the aft wing. Further, Fig. 18 indicates the best lift-to-drag ratio occurs near a 5° angle of attack. As seen in Fig. 17, this occurs at a C_L of 1.18. The tangent to the drag polar in Fig. 19 confirms that the best L/D ratio occurs at about this lift coefficient. The high-drag values for twist down in the drag polar are again due to the separation above a −5° angle of attack, evident in Fig. 15.

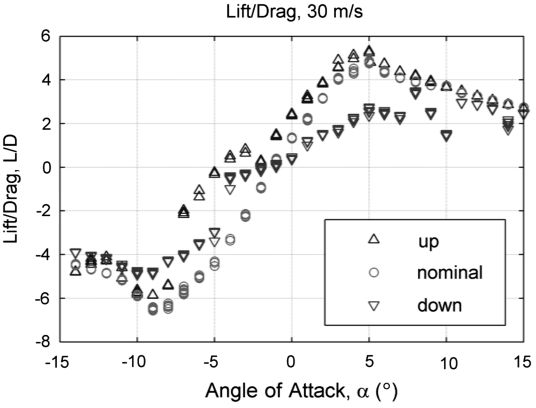

Fig. 18 Lift-to-drag ratio for twist up, down, and nominal configurations.

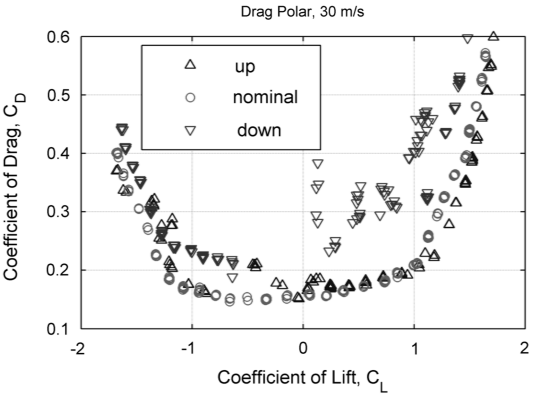

Fig. 19 Drag polar for twist up, down, and nominal configurations.

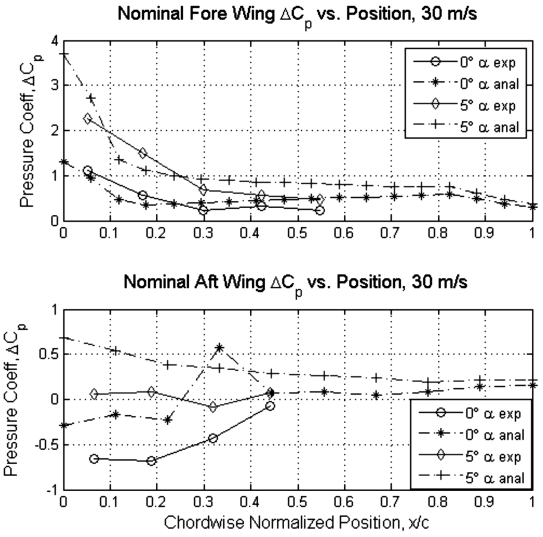

Fig. 20 Experimental and computational pressures for nominal wing configuration.

Twist down apparently leads to separation above a −5° angle of attack. An improved aerodynamic design is needed to avoid severe restriction of the flight envelope. Nominal and twist-up minimum drag appears at about −4 or −5° angles of attack, which is also not ideal. An improvement to this design would have $C_{D\min}$ at a C_L greater than zero. The trends in the experimental force and moment data indicate that there is an extremely tight angle-of-attack range in which the vehicle is not in a high-drag or flow separation region.

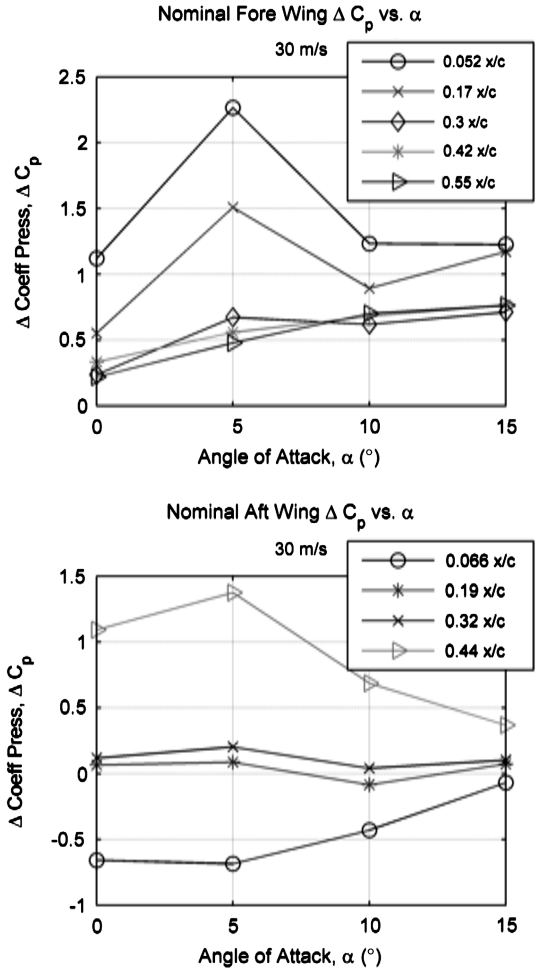

Fig. 21 Experimental pressures vs angle of attack for nominal wing configuration.

Table 4 Maximum standard deviation and range of Schenck balance lift and moment measurements

Twist, °	Speed, m/s		Fx, N	Fz, N	My, N·m
Nominal (0)	20	**Std. Dev.**	**0.091**	**0.156**	**0.022**
		Max.	−0.12	13.67	1.52
		Min.	−10.93	−12.61	−1.56
	30	**Std. Dev.**	**0.445**	**2.356**	**0.120**
		Max.	3.58	75.83	3.85
		Min.	−24.15	−64.66	−3.42
	40	**Std. Dev.**	**0.187**	**0.500**	**0.082**
		Max.	0.64	63.35	0.97
		Min.	−9.94	−47.44	−4.09
	50	**Std. Dev.**	**5.859**	**6.428**	**0.805**
		Max.	3.12	103.44	5.24
		Min.	−17.66	−72.73	−3.92
Twist up (+15)	20	**Std. Dev.**	**0.064**	**0.115**	**0.018**
		Max.	0.41	17.52	0.58
		Min.	−1.93	−16.04	−0.08
	30	**Std. Dev.**	**0.900**	**0.262**	**0.033**
		Max.	1.52	38.54	1.8
		Min.	−6.37	−36.11	−1.73
	40	**Std. Dev.**	**1.853**	**1.576**	**0.110**
		Max.	3.58	75.83	3.85
		Min.	−24.15	−64.66	−3.42
	50	**Std. Dev.**	**7.163**	**2.990**	**0.291**
		Max.	12.46	90.14	5.2
		Min.	−49.41	−78.72	−3.77
Twist down (−15)	20	**Std. Dev.**	**0.048**	**0.092**	**0.015**
		Max.	41.92	46.18	7.9
		Min.	−4.32	−14.01	−9.18
	30	**Std. Dev.**	**0.114**	**0.386**	**0.041**
		Max.	40.18	64.98	7.16
		Min.	−6.81	−32.03	−10.13
	40	**Std. Dev.**	**0.148**	**0.435**	**0.077**
		Max.	37.4	90.65	6.09
		Min.	−7.69	−53.73	−11.41
	50	**Std. Dev.**	**6.533**	**1.953**	**0.505**
		Max.	4.84	93.51	0.02
		Min.	−22.02	−73.75	−7.08

Thus, the airfoil design is critical to prevent separation at such an early stage. In addition, shrouding the twist mechanism at the aftwing root joint is important to decrease the stall, explicitly evident in the aftwing twist-down configuration.

B. Computational and Experimental Test Pressure Results

In addition to force and moment data, the pressure was measured at the midsection of each of the wings. The intent was to use it to help explain phenomena in the force and moment data that may not be fully understood. Computational results produced in MSC/Nastran from the aerodynamic panel model are compared with experimental data in Fig. 20 for the 30 m/s nominal wing (zero twist) case. Pressures match reasonably well for the forward wing but do not match well for the aft wing. Experimental pressure dropped slightly more than predicted past the quarter-chord on the forward wing. Aftwing pressure was greatly overpredicted, possibly due to poor wake modeling, leading to neglected downwash from the forward wing. The drastic change in pressure measured toward the leading edge on the forward wing (top plot in Fig. 21) and on the aft wing (bottom plot in Fig. 21) between 5 and 10° angles of attack accounts for the discontinuity in C_{My} at a 5° angle of attack (Fig. 14).

V. Conclusions

Measurements of force, moment, and pressure were taken in a wind-tunnel experiment for a 1:38 scale model of a joined-wing sensorcraft. The goal was to investigate the feasibility of incorporating flexible twist for pitch control in the design of a high-altitude long-endurance aircraft. Flexibility was designed into the full-scale model by modifying the aftwing ribs and creating a spanwise slit to reduce the torque required to twist the aft wing at the root up to ±15°. The resulting, deformed OML was used to fabricate two scaled, rigid aft wings configured in the deformed state, as well as a nominal aft wing in the undeformed state. Unfortunately, the size and speed restrictions of the wind tunnel prevented achieving a scaled Reynolds number. As a result, flow separation effects were evident, compounding possible interference effects of the forward wing on the aft wing.

The lift coefficient did not suffer from separation or interference effects at the nominal (no twist) condition. Once corrected for a zero angle of attack to compensate for the neglected camber in the aerodynamic panel model, the experimental lift coefficient compared favorably to the computational prediction. The calibration for the zero-lift angle of attack and the center-of-pressure moment arm found, based on the lift and moment curves, will be useful for the validity of the present doublet-lattice aerodynamics for the next-generation design. Lift remained linear with respect to the angle of attack from about −10 to +10° effective angles of attack. Stall did not occur within the ±15° angle-of-attack region of this experiment for the nominal configuration, but it appeared imminent. The pitching moment was consistent for the nominal configuration below 50 m/s, remaining linear from about −7 to +8° effective angles of attack. At 50 m/s, the moment curve was highly nonlinear.

Concentrating on the most repeatable measurements at 30 m/s, the pitch-up twist condition showed the expected pitching moment effectiveness in the roughly linear region from about −10 to +5° angles of attack. Outside this region, separation effects negated the predicted change in moment. In contrast, interference and separation effects were pervasive for the twist-down configuration, negating practically all of the predicted change in moment.

In summary, by plotting the coefficient of the pitching moment vs the angle of attack for three aftwing twist conditions, the experimental results demonstrated that pitch control effected by aftwing twist was effective in the twist-up condition over a range of

approximately 20° angles of attack. Outside this range, and for the twist-down condition, separation effects, possibly exacerbated by interference of the forward wing on the aft wing, negated the predicted pitching moment effectiveness. The unshrouded aftwing root connection may have also contributed to flow separation on the aft wing. Recommendations for future experiments include shrouding the aftwing root, the use of a trip wire in the boundary layer to control laminar-to-turbulent transition at the lower Reynolds numbers, or conducting the experiments well above the critical Reynolds number for designing joined wings without laminar flow control. Finally, measuring pressure, force, and moment for isolated forward and aft wings before taking measurements on the joined wing is advised in order to determine interference effects.

Acknowledgments

The authors thank Raj Nangia for his helpful analytical interpretation of the data. The authors are indebted to Jenner Richards from the University of Victoria for the drawing expertise used to build the model. The authors also thank the reviewers for their insightful comments.

References

[1] Martinez, J., Flick, P., Perdzock, J., Dale, G., and Davis, M., "An Overview of SensorCraft Capabilities and Key Enabling Technologies," 26th AIAA Applied Aerodynamics Conference, AIAA Paper 2008-7185, Aug. 2008.

[2] Wolkovitch, J., "The Joined Wing: An Overview," *Journal of Aircraft*, Vol. 23, No. 3, March 1986, pp. 161–178. doi:10.2514/3.45285

[3] Kroo, I. M., Gallman, J. W., and Smith, S. C., "Aerodynamic and Structural Studies of Joined-Wing Aircraft," *Journal of Aircraft*, Vol. 28, No. 1, Jan. 1991, pp. 74–81. doi:10.2514/3.45994

[4] Smith, S. C., Cliff, S. E., and Kroo, I. M., "The Design of a Joined Wing Flight Demonstrator Aircraft," AIAA/AHS/ASEE Aircraft Design, Systems and Operations Meeting, AIAA Paper 1987-2930, Sept. 1987.

[5] Tyler, C., Schwabacher, G., and Carter, D., "Comparison Of Computational and Experimental Studies for a Joined-Wing Aircraft," AIAA Paper 2002-0702, Jan. 2002.

[6] Corneille, J., and Franke, M., "Wind Tunnel Tests of a Joined-Wing Missile Model," AIAA Paper 2000-0938, Jan. 2000.

[7] Blair, M., Canfield, R., and Roberts, R., "A Joined-Wing Aeroelastic Design with Geometric Non-Linearity," *Journal of Aircraft*, Vol. 42, No. 4, July–Aug. 2005, pp. 832–848. doi:10.2514/1.2199

[8] Pope, A., *Wind Tunnel Testing*, 2nd ed., Wiley, New York, 1954, p. 3.

[9] Bisplinghoff, R., Ashley, H., and Halfman, R., *Aeroelasticity*, Dover, New York, 1996, p. 710.

[10] Sitz, J., "Aero-Structural Coupling and Sensitivity of a Joined-Wing Sensor-Craft," M.S. Thesis AFIT/GAE/ENY/04-J12, Air Force Inst. of Technology, Wright-Patterson AFB, OH, June 2004.

[11] Kimler, F., and Canfield, R. A., "Structural Design of Wing Twist for Pitch Control of Joined Wing SensorCraft," 11th AIAA/ISSMO Multidisciplinary Analysis and Optimization Conference, AIAA Paper 2006-7134, Sept. 2006.

[12] Roberts, R., "Sensor-Craft Analytical Certification," M.S. Thesis AFIT/GAE/ENY/03-06, Graduate School of Engineering, Air Force Inst. of Technology, Wright-Patterson AFB, OH, March 2003.

[13] Anderson, J. D., Jr., *Introduction to Flight*, 2nd ed., McGraw–Hill, New York, 1985, p. 372.